THE ASTROPHYSICAL JOURNAL, 361:514–526, 1990 October 1

INDEPENDENCE OF SHORT TIME SCALE FLUCTUATIONS OF QUASI-PERIODIC OSCILLATIONS AND LOW-FREQUENCY NOISE IN GX 5−1

J. P. NORRIS, P. HERTZ, AND K. S. WOOD
E. O. Hulbert Center for Space Research, Naval Research Laboratory
B. A. VAUGHAN AND P. F. MICHELSON
Physics Department, Stanford University
AND
K. MITSUDA AND T. DOTANI
Institute for Space and Astronautical Science
Received 1989 December 22; accepted 1990 April 2

ABSTRACT

We examine the short time-scale variability in the X-ray flux of the quasi-periodic oscillations (QPOs) and low frequency noise (LFN) in GX 5−1. The data are drawn from a *Ginga* observation while the source was on the horizontal spectral branch. During the observation, the total X-ray intensity, 1.9 counts cm^{-2} s^{-1}, and QPO centroid frequency, 24 Hz, were nearly stationary. We apply several new statistical tests for short time-scale variability and correlation among power spectral components to the GX 5−1 data in order to determine whether the QPOs are carried by LFN shots, as required by the beat-frequency modulated-accretion model. On time scales of ~1 s, significant, but uncorrelated, QPO and LFN Fourier power fluctuations are evident. Simulations of QPOs carried by LFN shots show significant QPO–LFN correlations for low shot rates, whereas in simulations of models with shot rates greater than 100 Hz the underlying relationship is masked by the intrinsic noise bias manifested by overlapping shots. However, other tests reveal the shot nature of the LFN when applied to simulations with shot rates as high as ~400 Hz: the mean intensity on a 1 s time scale is positively correlated with LFN power, and the intensity skewness is positive. For GX 5−1 the mean intensity on a 1 s time scale is uncorrelated with LFN power, and the intensity skewness is consistent with LFN shapes distributed symmetrically about the mean.

In summary, there is no indication in the GX 5−1 data that QPOs are carried by positive shots with lifetimes of ~1 s or less, whereas our simulations show that some tests would reveal the shot nature of the LFN and its relationship to the QPO if it were present. Instead, the results are consistent with a picture of QPOs produced independently of an intensity-symmetric LFN component.

Subject headings: stars: individual (GX 5−1) — stars: neutron — X-rays: binaries

I. INTRODUCTION

Low-mass X-ray binaries (LMXBs) contain a compact primary, typically a neutron star, which accretes matter from a Roche-lobe filling, low-mass secondary. Many of the brighter LMXBs have been observed to produce fast, low-amplitude quasi-periodic oscillations (QPOs) of their X-ray flux. Although it is not clear how many mechanisms are required to explain all of the observed QPOs, a coherent observational picture is beginning to emerge for a large subset of QPO sources. At least six LMXBs, referred to as *Z*-sources, exhibit up to three possibly distinct QPO modes (Hasinger and van der Klis 1989), and each QPO mode is associated with a different spectral state of the LMXB. For *Z*-sources, the characteristics of QPO peaks in Fourier power spectra are mode dependent and exhibit centroid frequencies ν from ~2 to ~50 Hz and (FWHM) widths $\Delta\nu/\nu$ from ~0.1 to more than 2. A mode-dependent noise component, which rises exponentially at low frequencies ($\nu < 1$–10 Hz), is also observed in the Fourier power spectra of QPO sources and is referred to as low frequency noise (LFN). Amplitudes of the incoherent waveforms which give rise to the QPO peaks are small, typically a few percent. In consequence, individual oscillations are imperceptible with present instruments (exceptional case: the Rapid Burster). QPO observations and theories have been extensively reviewed by many authors, including Lewin, van Paradijs, and van der Klis (1988), Stella (1988), Lamb (1988), and van der Klis (1989*a*).

Out of six *Z*-sources, QPOs have been observed from four sources while they were in the horizontal branch spectral state where spectral hardness is, to first-order, independent of intensity and strong correlations between QPO centroid frequency and source flux are evident (GX 5−1: van der Klis *et al.* 1985; Cyg X−2: Hasinger *et al.* 1986; GX 17+1 and GX 340+0: Hasinger and van der Klis 1989). In GX 5−1 and Cyg X−2, Fourier power in the QPO and LFN is strongly correlated on intermediate time scales of a few minutes (van der Klis 1986).

A beat-frequency modulated-accretion (BFMA) model has been developed to explain the strong correlations observed in GX 5−1 and other sources exhibiting horizontal branch QPOs (Alpar and Shaham 1985, elaborated in Lamb *et al.* 1985, and Shibazaki and Lamb 1987; also see Shibazaki, Elsner, and Weisskopf 1987 and Elsner, Shibazaki, and Weisskopf 1987). The beat frequency, which is manifest as the QPO peak in Fourier power spectra, is postulated to arise from the difference between the instantaneous Keplerian orbital frequency of clumped accreting matter—which enters the transition zone of a moderately strong magnetosphere ($B \sim 10^9$–10^{10} G) from the accretion disk—and the neutron star rotation frequency (~100 Hz). The X-ray temporal signature of this clumped matter, generated upon encountering the

stellar surface, is the LFN (or a subcomponent thereof). The LFN envelope is modulated (chopped) at the beat frequency as it leaves the transition zone.

The BFMA model views a portion of the X-ray flux as shot envelopes (from the accretion of clumped matter) carrying periodic pulsations (from the chopping of the clumps at the beat frequency). These shots are in addition to the persistent X-ray emission from essentially steady accretion; the proportions of the total X-ray flux contributed by these components (shots and steady emission) are currently unconstrained by observations or theory. The detailed physics involved in X-ray emission under the BFMA model is not well understood at this time; the result is a large number of free parameters for the mathematical representation of the BFMA model. Parameters describing the shots include the shot rate, the shape of the shot envelope, the distribution of the shot amplitudes, and the sign of the shot. Positive shots result from the accretion of a clump, whereas negative shots come from a hole (or region of lower mass density) in the accretion stream. Any of these parameters can be correlated with the persistent emission.

The QPO is described by its underlying frequency, the lifetime of individual QPO wave trains (related to the coherence length in cycles: $N_{cyc} = \nu_{qpo}\tau_{qpo}$), the amplitude of the pulsed component and its dependence on shot amplitude, and the phase coherence memory between shots. This latter property, referred to as shot clustering by Shibazaki and Lamb (1987), results in higher QPO peaks in the Fourier power spectra at high shot rates. With some degree of coherence memory, the pulsations in overlapping shots would add with partial coherence and have more total power, and the resulting QPO spectral feature would be narrower for a given LFN shape. An additional parameter which can affect the width of the QPO feature is the degree of QPO frequency drift or modulation (FM) which occurs while a shot crosses the transition region (Lamb *et al.* 1985; Shibazaki and Lamb 1987). We do not treat the effects of FM in this paper. Preliminary modeling has determined that the width of the QPO peak is not very sensitive to the range of FM expected in the BFMA model for the QPO centroid frequency (24 Hz) in this observation (Norris *et al.* 1989*b*): the presence of FM cannot be excluded, neither can it be affirmed with any confidence. Consequently, the parameter most highly correlated with FM—coherence length (increasing FM requires increasing the coherence in order to keep the QPO width constant)—is not substantially affected if FM modeling is not included.

Figure 1 schematically illustrates several kinds of time series of overlapping LFN shots which carry QPOs, as described above. A small number of shots is shown for clarity; at much higher shot rates the correlation between QPO and LFN strength is not obvious to the eye. The low counting statistics of real data render the individual QPO cycles and LFN shots indiscernible. In Figure 1*a* the positive intensity shots have exponentially decaying shapes, and the QPO waveform is incoherent from shot to shot; Figure 1*b* shows a similar picture except that the QPOs retain phase memory between shots, and thus their amplitudes add coherently. The same two variations for rectangular shot shapes are shown in Figures 1*c* and 1*d*. A distinction between the next two cases is relevant for models which include negative shots and QPO coherence memory. Figures 1*e* and 1*f* show examples where the positive shots have phases shifted by 180° and 0°, respectively, relative to the negative shots. As the shot rate increases, case *e* produces less QPO power, rather than more as in case *f*. Any QPO mechanisms with coherence memory which result in shots of "negative flux" with reversed phase are thus effectively excluded (the BFMA model does not explicitly predict such phase-reversed behavior). The QPO amplitude is always some proper fraction of the LFN amplitude since the shot carries the QPO. Cases *a*–*d* are modeled in this paper.

Correlations between low signal effects, such as those studied here, can be masked by biases resulting simply from noise. There are possibly two different noise biases present in QPO data. The first is Poisson noise. The stochastic nature of the data can result in amplitude (and other) correlations even where none is present—fluctuations in the data necessarily contribute to the measured LFN and QPO. The second bias is

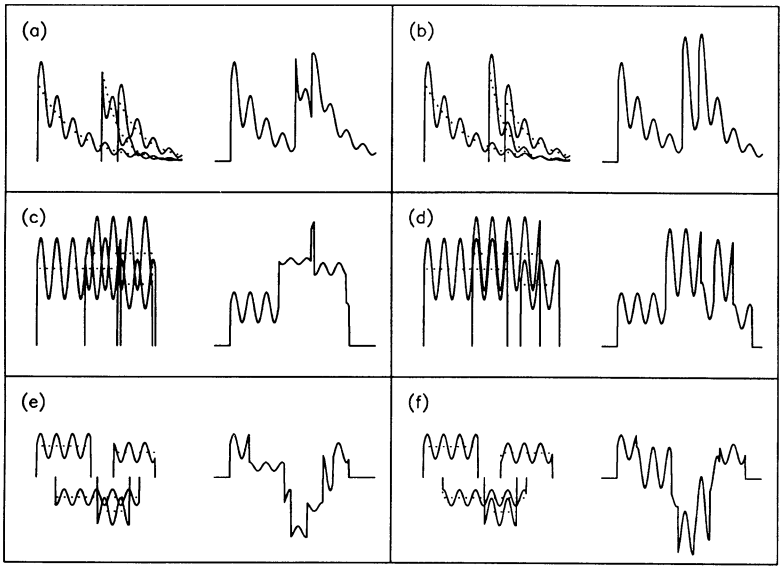

FIG. 1.—Schematic illustrations of overlapping LFN shots carrying QPOs. (*a*) Positive intensity shots with exponentially decaying shapes and incoherent QPOs from shot to shot; (*b*) same as (*a*) except QPO phase coherence (memory) across shots. (*c*–*d*) Rectangular shot shapes, as in (*a*) and (*b*), respectively. (*e*-*f*) Both positive and negative shots with phase memory, positive shot phases shifted by 180° and 0°, respectively, compared to negative shot phases.

intrinsic to shot models. For example, one can construct a BFMA model where the amplitudes of the QPO and shot are independent. However, since only the product of these amplitudes (the shot carries the pulsations) is observed, analyses of the type we describe here show some degree of correlation at short time scales. As the shot rate increases, however, the correlation decreases (especially when integrating over time scales much longer than shot lifetimes) since overlapping shots of varying amplitudes tend to average out the individual amplitude fluctuations. We thus rely on simulations of shot models to calibrate the noise bias in our data.

According to the BFMA model as presently formulated (Lamb *et al.* 1985; Shibazaki and Lamb 1987), the fundamental mechanism of QPO resulting from modulation of the LFN shot lends itself to various short time scale tests. Small (large) shot amplitudes necessarily imply small (large) QPO amplitudes (for each shot). If this version of the BFMA model is correct, QPO and LFN amplitudes should be found to be correlated, at some level, on the time scale of the shot lifetimes. Alternative mathematical formulations (which may seem physically artificial), e.g., in which the QPO amplitude varies inversely with the LFN amplitude, may be constructed. In this article we investigate QPO and LFN activity in GX 5−1 on the short time scales relevant to the proposed mechanism of the BFMA model. While individual QPO waveforms in the present observation are still overwhelmed by low counting statistics, *Ginga*'s Large Area Counter (LAC) instrument affords sufficiently high count rates to permit a statistical search for correlations between QPO and LFN fluctuations.

In § II we describe the GX 5−1 observations and a range of simulations, all of which reproduce the average GX 5−1 power spectrum, i.e., the variance as a function of frequency; the simulations differ, effectively, in degree of correlation among the Fourier phases. In § III we show that significant LFN and QPO power fluctuations occur on short time scales in GX 5−1. We describe a test for correlation between LFN and QPO power fluctuations and show that LFN and QPO power are uncorrelated on time scales comparable to the shot lifetimes in GX 5−1. We also investigate shot amplitude distributions showing that the third moment (skewness) of the intensity in GX 5−1 vanishes on LFN time scales and that the local mean is uncorrelated with LFN power. In contrast, in simulations the piling up of shots produces positive skewness, and random variations in shot rate produce a correlation of local mean with LFN strength. Finally in § IV we discuss the import of our results for QPO phenomenology in general and the BFMA in particular. In order for the BFMA model to remain viable, (1) shot profiles must be distributed such that approximately equal positive and negative excursions about the mean intensity occur, (2) the majority of the total X-ray flux must arise from the shots rather than from a steady component, and (3) shot rates higher than predicted must somehow operate, so that the intrinsic noise bias masks any possible correlations.

II. OBSERVATION AND SIMULATIONS OF GX 5−1

a) Observation

We have analyzed data obtained during an observation of GX 5−1 on 1987 April 20 with the *Ginga* LAC instrument (Makino 1987; Turner *et al.* 1989). At the time of the observation the source was on the horizontal spectral branch, which for GX 5−1 means that spectral hardness is approximately independent of intensity and QPO centroid frequency is strongly correlated with intensity (van der Klis *et al.* 1985). Four energy channels are available at ~2 ms (1/512 s) resolution. We summed the two low-energy and two high-energy channels from the LAC A and B counters (total area ~4000 cm^2) to produce counting rates in overlapping energy bands, 0.8–7.9 keV and 5.7–18.0 keV. The average rates in these two bands are 12.7 and 4.4 counts per 2 ms bin, respectively. The entire analysis was performed for the two bands separately and combined; results are similar in all three cases. The details are discussed here only for the combined counting rates as these are more significant.

Figure 2 illustrates the combined data in the time domain, uncorrected for collimator movement, and binned to 8 s. *Ginga*'s attitude determination is uncertain to ~5′ and maximum measured pointing drift was on the order of ~0°.04. As a result the plotted rate differs from the incident intensity by ~3.5%–4.5% with variations occurring on a time scale of 5–10 minutes. We selected the first 2304 s of data (including two 4 s intervals containing zero data) in Figure 2 because the source intensity is relatively stable. This affords the possibility of studying fluctuations in the QPO and LFN amplitudes in the statistical aggregate without complicating effects (e.g., variations in QPO centroid frequency, LFN slope, etc.). Averaged on an 8 s time scale, fluctuations in the local mean are such that 85% of the intervals fall within 2% of the global mean. Some of this 2% variation arises from collimator motion, for which the uncertainty in pointing attitude induces variations of the same order; thus, much more precise knowledge of intrinsic intensity is unavailable. From Figure 5 of van der Klis *et al.* (1985), we estimate that, if all the intensity variation were intrinsic to the source, variations of ±2% would imply variations in QPO centroid frequency of ±2.25%, QPO power of ±3.6%, and LFN power of ±2.3%.

Figure 3 illustrates the combined data in the frequency

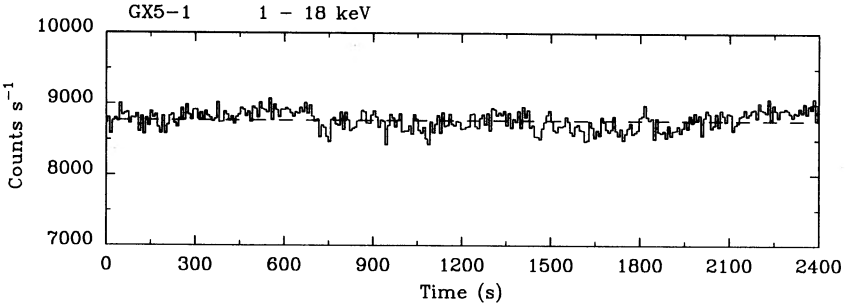

FIG. 2.—LAC counting rate for portion of 1987 April 20 observation of GX 5−1 in the energy band 0.8–18.0 keV. Start UT 18:46:33. Dashed line is mean of first 2304 s. Resolution is 8 s.

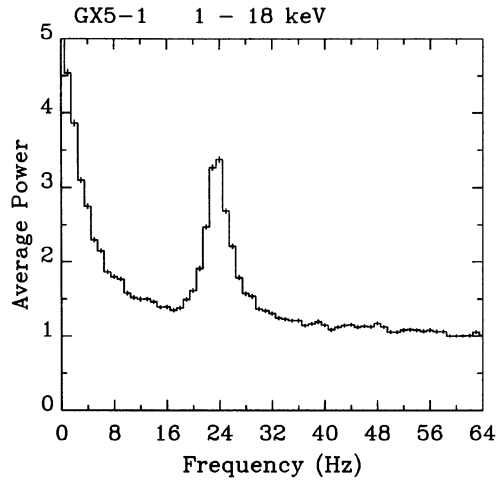

FIG. 3.—Average Fourier power spectrum for first 2304 s of Fig. 2. Resolution is 1 Hz per frequency channel.

domain. We have averaged the power spectra of 2296 512 bin fast Fourier transforms (FFTs). Because the QPO centroid frequency is very nearly at 24 Hz for the entire data sample, the detailed shape of the power spectrum in Figure 3 is characteristic of spectra on an intermediate time scale of a new minutes. The normalization is derived from the average of (essentially) Poisson-distributed white noise in the frequency range 193–256 Hz. Since the count rate is nearly constant, the global mean of the white noise for the whole data set is used for normalizing individual FFTs; this procedure errs on the conservative side by avoiding introduction of spurious power fluctuations which result from low statistics of short interval averages. Our normalization is unity rather than two, but is consistent with other treatments (Leahy *et al.* 1983; van der Klis 1988).

b) Simulations

In analyses where the signal-to-noise ratio (S/N) is relatively low, a large noise bias is present which tends to level any correlation among parameters. As discussed in § I, two different kinds of noise bias may contribute to the problem of exploring the QPO–LFN relationship: that resulting from the Poisson noise, and the intrinsic noise bias of models with high shot rates. The problem is ameliorated in our treatment by employing a long data set with essentially stationary temporal behavior, as described in the previous section. Although noise does tend to level correlations, residual trends are potentially detectable if enough data is used since decreased error bars on data and models result.

Simulated data sets were constructed in the time domain for the purpose of calibrating the significance of results found for GX 5−1. With models we are able to quantify the sensitivity of tests for correlations of power spectrum descriptors. We fully evaluated a range of simulations in which (1) shots have rectangular or exponentially decaying shape; (2) shots have positive intensity profiles; (3) the QPO wave train associated with a given shot persists the entire length of the shot; (4) Gaussian distributions were used for shot and QPO amplitudes, coherence length; (5) during a given shot the QPO amplitude is a constant proper fraction of the shot amplitude. Considerable attention was given to the effects of possible QPO coherence memory between shots. Some models were constructed with positive and negative shot distributions in order to demonstrate the effects on skewness.

These limitations do not overly compromise the generality of the interpretations for several reasons. First, rectangular and exponential shot shapes define a range of possible LFN behaviors. In addition, *the piling up of shots at high shot rates produces a resultant LFN waveform with arbitrary frequency content*; unless individual shots have rather complex shapes, piling up is likely to be the dominant amplitude modulation effect for realizations similar to BFMA models (which can have shot rates as high as ~300 Hz for sinusoidal QPO, and lifetimes of ~0.05–5 s; Lamb *et al.* 1985). It is probably for the same reason that the results are relatively insensitive to the exact form of the distributions for shot and QPO amplitudes; uniform distributions gave end results similar to Gaussian distributions.

Second, we found similar degrees of QPO–LFN correlation for models with positive-only, or negative-only, shots and models with both positive *and* negative shots; therefore, the results presented here for positive-only shot models apply to all three kinds. The reason the correlations are so similar for a given shot rate is the same as that described above for shot shape: high shot rates give rise to a relatively arbitrarily shaped waveform, at least as far as the QPO–LFN relationship is concerned. The primary difference between the two kinds of models is the skewness on LFN time scales.

Finally, we found that only shot models incorporating some degree of QPO coherence memory can fit GX 5−1 power spectra averaged on a 1 s time scale. That is, we were successful in fitting the GX 5−1 QPO relative to the LFN strength only by enforcing some degree of QPO coherence memory across shots (clustering) which pile up in a given time interval—the LFN distribution extends too high in frequency to produce a narrow enough QPO feature otherwise. Since some QPO coherence memory is required across several overlapping shots, the constraint that QPOs persist the entire length of a shot becomes a secondary concern in high shot rate models. There is an important effect associated with the possibility of a duty cycle for QPOs which is not quantified here: a less than 100% QPO duty cycle during a shot would require that intervals of relatively stronger QPO within the shot occur, a constraint that must be met by physical models. Also, the BFMA model has sufficient freedom to invoke "swarms" of clustered QPO waveforms (Shibazaki and Lamb 1987), each swarm having *incoherent* QPO contents relative to another. We did not model such swarms. The primary effect of including "swarming" would be to *increase* the required QPO amplitude of the swarms, and therefore to increase the QPO/LFN correlation; the effect of swarming offsets that of clustering. Thus in both of these simplifications, our modeling fortuitously errs on the conservative side in that inclusion of such possible effects would only serve to increase the observable degree of correlation between QPO and LFN.

Construction of the simulated data sets proceeded as follows. For each model a shot rate and shot clustering fraction were selected as the independent parameters, then the remaining parameters were adjusted until the model's average power spectrum accurately fitted that of the GX 5−1 data (Fig. 3). A successful fit reproduces the GX 5−1 variance as a function of frequency but does not address the relationship between Fourier phases. Shots were produced with a uniformly random distribution of start times and with uncorrelated durations. The LFN power spectrum shape is well described in the range

~1–10 Hz by an exponential function. For models with rectangular shots a Gaussian distribution of LFN lifetimes with mean of 0.071 s and standard deviation of 0.022 s adequately reproduced the LFN e-folding frequency scale; for exponential shots, lifetimes in the range 0.053–0.046 s with deviations of ~0.010–0.012 s were required. The shot amplitude was then adjusted until the power level matched that of Figure 3 in the LFN range. Exponential models required approximately twice the (initial) shot amplitude as did rectangular models for a given shot rate, reflecting the lower average amplitude of the exponential shape. The fitted ratio of QPO amplitude to LFN amplitude depends largely upon amount of QPO coherence memory and less on shot shape.

A sinusoid with frequency fixed at 23.875 Hz reproduced the GX 5−1 QPO centroid for the coherence length range required. The shot amplitude, QPO amplitude, and coherence length were selected from Gaussian distributions with associated widths. By adjusting these distributions, a fit was obtained to the QPO width and strength. For the clustered component, where the QPOs are coherent across overlapping shots, the resulting intensity time series can be expressed as the sum of the mean and a point by point product of a resultant shot shape function and a QPO amplitude function:

$$I_1(t_i) = \mu + \sum_n \{A_{\text{shot},n} \prod [(t_i - t_n)/\tau_n - \tfrac{1}{2}]\} \times \prod [(t_i - t_m)/\tau_m - \tfrac{1}{2}][1 + A_m \sin (t_i \Omega_{\text{QPO}} + \phi_m)] , \quad (1)$$

where μ is the mean, and $\prod(x)$ is the rectangle function (unity for $|x| < \frac{1}{2}$, zero otherwise); for exponential shot models, the shot shape $\prod$ function is replaced by $\exp [(t_i - t_n)/\tau_n]$. The LFN parameters are n, the shot number; $A_{\text{shot},n}$, shot amplitude; t_n, shot start time; τ_n, shot lifetime. For each interval m during which overlapping shots' QPO contents are coherent, the independent QPO parameters are A_m, QPO amplitude; t_m, coherence start time; τ_m, coherence length; and ϕ_m, start phase. For the nonclustered component, the QPO contribution is incoherent from shot to shot and is therefore described by

$$I_2(t_i) = \mu + \sum_n \{A_{\text{shot},n} \prod [(t_i - t_n)/\tau_n - \tfrac{1}{2}] \times [1 + A_{\text{QPO},n} \sin (t_i \Omega_{\text{QPO}} + \phi_m)]\} , \quad (2)$$

where ϕ_m is regenerated only if the shot duration is longer than the coherence length. The clustered and nonclustered components were then summed and the time series renormalized to the GX 5−1 mean.

Finally, in order to simulate the fluctuations of photon counting statistics, the simulated time series was Poisson distributed about the instantaneous intensity. Table 1 lists the parameter values for some models which successfully reproduce the GX 5−1 power spectrum and which we discuss in detail. The tabulated shot amplitudes are the renormalized ones.

Note that for the clustered component, an input QPO envelope which persists over an interval of QPO coherence is multiplied (and therefore bounded) by the instantaneous LFN waveform (resultant sum of shots). Our code includes the option for producing models where the input QPO envelope has varying amplitude (not associated with shot shape). In all models described here the input QPO amplitude is constant during a coherence interval (clustered component) or during a single shot (nonclustered), and therefore all amplitude modulation of the QPO arises from the LFN shape.

As the shot rate increases, individual shots necessarily must have lower amplitudes to fit the data. For sufficiently high shot rates, overlapping shots give rise to an arbitrarily shaped LFN waveform with enough varying frequency content that the relationship between QPO and LFN can be effectively masked on a given time scale: integrations (e.g., 1 s FFTs) over many shots, each of which carries a relatively low amplitude QPO, average out the rapid LFN fluctuations.

The 28 and 100 Hz shot rate models in Table 1 were constructed to demonstrate that, given enough data, the relationship between LFN and QPO in shot models can be discernible. The 400 Hz models were selected to compare with some variants of the BFMA model (Lamb *et al.* 1985). As we shall see in the next section, at 400 Hz shot rates the intrinsic noise bias is too high for one of our tests to be sensitive to the QPO–LFN relationship. At least two recourses are possible which counteract the increased bias: the use of (1) longer data intervals in order to shrink error bars, and (2) algorithms which explore the QPO–LFN relationship on shorter time scales. Some successful alternative algorithms are suggested in § IV.

III. ANALYSIS

a) QPO and LFN Power Distributions

Although the individual waveforms of the QPO are generally indiscernible, one may still ask: Does the observed ensemble of QPO amplitudes differ from that expected if the QPO amplitude were constant, and if so, then by how much? A difference would not necessarily imply amplitude variations, but could reflect phase modulation, or a combination of effects. In the presence of photon counting noise, the expected QPO power fluctuations may be estimated, assuming a constant QPO amplitude, adapting the treatment of Groth (1975) to cover QPOs. Equation (16) of Groth expresses the probability of finding power less than or equal to a given power (P),

TABLE 1

MODEL PARAMETERS

Model[a]	Shot Rate (Hz)	LFN[b] τ^{-1} (Hz)	Shot Amp/DC	QPO Amp/Shot Amp	Coherence Length (cycles)	Shot Clustering Percentage[c]
R400	400	14 ± 4	0.011 ± 0.003	0.400 ± 0.090	3.40 ± 0.80	50%
R100	100	14 ± 4	0.023 ± 0.005	0.410 ± 0.090	3.35 ± 0.80	100%
R28	28	14 ± 4	0.043 ± 0.009	0.720 ± 0.140	3.75 ± 0.90	100%
E400	400	20 ± 4	0.019 ± 0.005	0.550 ± 0.120	4.00 ± 0.95	50%
E100	100	22 ± 4.5	0.041 ± 0.010	0.930 ± 0.170	5.10 ± 1.20	50%

[a] Rectangular shots: models R28, R100, and R400; exponential shots: models E100 and E400.
[b] Inverse of shot lifetime.
[c] Percentage of shots with mutually coherent QPO wave trains.

assuming that a coherent signal of constant power (P_s) is present and that the power spectrum is normalized such that the expected power from Poisson fluctuations is unity,

$$f_n(P; P_s) = 1 - \exp\left[-(P + P_s)\right] \sum_{m=0}^{\infty} \sum_{k=0}^{m+n-1} P^k P_s^m/(k!m!)$$

for $2n$ degrees of freedom (n power spectral channels). The average QPO powers per channel (Fig. 3) were used as the hypothetical constant signals. In other words, we measure the QPO fluctuations against the null hypothesis that the QPO bump in Figure 3 is comprised of a sum of coherent sinusoids at frequencies 22, 23, ... 26 Hz, with appropriate constant amplitudes. Indeed such a simulation, when divided into 1 s FFTs, precisely reproduces the shape of the QPO bump. Of course, longer FFTs of coherent signals would yield higher power peaks at discrete frequencies, unlike the actual QPO. Many alternative hypotheses can be tested, e.g., those in which various QPO amplitude distributions are assumed. For present purposes we estabish that QPO and LFN fluctuations do occur and then show that they are uncorrelated to within measurement errors.

In order to determine the appropriate level of signal to ascribe to the QPO feature, we fitted the average power spectrum of Figure 3 using a functional form comprised of an exponential for the LFN, a Lorentzian for the QPO, and unity for Poisson noise (van der Klis *et al.* 1985). The fit was slightly low in the valley between the LFN and QPO and at frequencies just above the QPO. Therefore, in order to realize the noise variance of unity as required by Groth (1975), both the expected and actual distributions were renormalized to take into account the local level of non–QPO power. This (close) approximation is just another way of adding a degree of freedom to fit the power spectrum, thus accounting for the fact that the QPO and the LFN are not exactly described by the chosen functional forms.

The solid line in Figure 4*a* is the expected (constant amplitude) cumulative distribution for the 24 Hz channel. Triangles denote the observed distribution of powers at 24 Hz for the 2296 1s FFTs. Cumulative observed powers below 4 are underabundant relative to the expected value, while above 4 the observed distribution is higher than expected. That the expected and observed distributions disagree is not surprising since the QPOs we study have short coherence lengths. Similar disagreements are found for all frequencies within the QPO feature, but not for control regions at 35 Hz (Fig. 4*a*, *dashed line and circles*) and higher frequencies.

Figure 4*b* illustrates where the excess power is concentrated. The differential curve gives the difference between actual and expected occurrences, times the value of the power bin, and normalized to total power, i.e., $dP(i) = 1 - N_{\rm exp}(i)/N_{\rm act}(i)$. The expected distribution has been evaluated every 0.2 unit, and then averaged over one unit of power; this results in a finite binning of expected powers which sufficiently precisely reflects a continuous binning. From the integral curve (integral from P

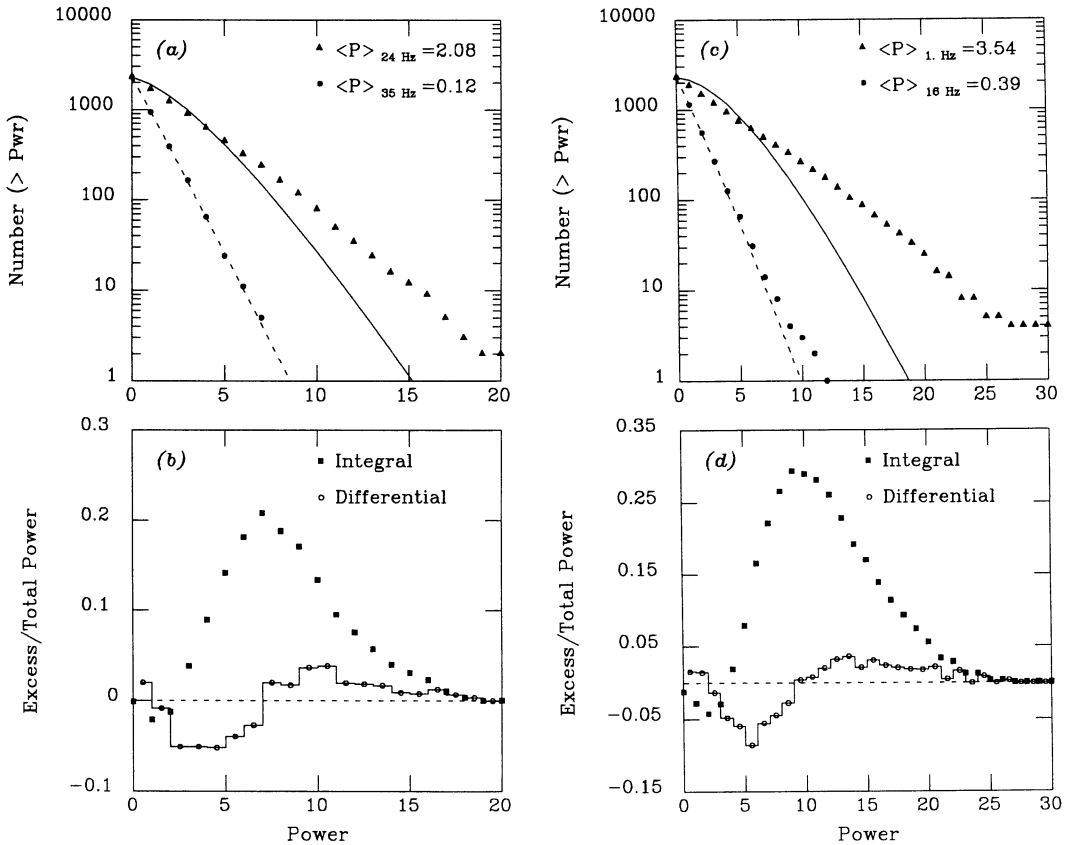

FIG. 4.—(*a*) Expected (constant amplitude) vs. observed cumulative distributions of QPO power. Solid line (*expected*), triangles (*observed*) at 24 Hz. Dashed line and squares for control channel at 35 Hz, on edge of upper QPO wing. (*b*) Differential and integral excess QPO power over expected as fraction of total power at 24 Hz. (*c*) Expected *vs.* observed cumulative distributions of LFN power at 1 and 16 Hz. (*d*) Same as (*b*) for LFN power at 1 Hz. $\langle P \rangle$ is average signal power (noise subtracted) per respective 1 Hz band.

to ∞) we see that occurrences with power 7 or greater constitute a 20% excess.

Figure 4*c* reveals a similar picture for the strong LFN at 1 Hz, and at 16 Hz near the minimum of the valley between QPO and LFN. Figure 4*d* shows that a 27% power excess at 1 Hz is associated with occurrences of powers greater than ~ 10.

We note that van der Klis (1989*b*) has suggested another null hypothesis, namely, that the QPO and LFN are pure noise. If one assumes that all the power under the QPO and LFN features is due to noise, then the expected and observed cumulative distributions actually agree: the observed power follows a χ^2 distribution scaled to the local average power. However, there are at least two reasons to believe that the QPO signal reflects some determinism. First, clearly the QPO spectral feature in GX 5−1 stands well above the ambient noise level on either side, suggesting that *some* effect of a deterministic nature gives rise to the high local power. Second, in some QPO data (e.g., a later portion of this GX 5−1 observation when the centroid frequency is higher) a very weak harmonic feature is seen at twice the fundamental QPO frequency. Thus, an accurate description of the QPO signal lies somewhere in between the pictures of pure noise and deterministic signal. We also note that if in fact a particular kind of QPO could somehow be demonstrated to be a pure noise process (see Scargle 1981), the BFMA model would not obtain in that case. Even if both the QPO and LFN arose from such processes it would still be appropriate to search for short time-scale correlations between these components, as we describe in the next section, since the processes need not be independent.

Disagreement between observed and expected distributions is found for ensembles of FFTs on time scales ranging from 0.25 s to ~ 8 s. As the time scale increases, i.e., for longer FFTs with the same sample bin size, the disagreement begins to vanish; for 16 s FFTs the expected (assuming constant signal) and observed cumulative distribution are in near agreement.

A most likely explanation for the agreement on longer time scales is as follows: The signals in the QPO and LFN bands are comprised of random noise and (time-varying) deterministic components. When the data is split into many short FFTs, those portions of the data set which have high (low) deterministic content and which fall entirely within the finite FFT length, tend to yield a large (small) spectral power. Some length FFT (near the coherence length for the QPO) would be optimal for characterizing the instantaneous QPO power—except that often the nearly coherent QPO wave trains would be split between adjacent FFTs. Much longer FFTs will contain many QPO wave trains, whose associated spectral power will be relatively diminished because of their mutual incoherence; thus on the longer time scales the noise component will dominate. In fact, the expected distributions for the van der Klis null hypothesis and the constant signal (plus noise) hypothesis will converge. This is because the amplitude of a constant, *coherent* signal that is required to fit the QPO signal becomes diminishingly small for longer data streams (coherent signals add power as the length of the data, incoherent ones as the square root).

Significant fluctuations which have distributions shaped similarly to those of Figure 4 are apparent when the data is divided into nine equal subintervals of 256 s apiece, indicating that the effect is not confined to one anomalous period. The fluctuations are also present in both the high- and low-energy data sets, with slightly lower significance in the latter. We conclude that, unless the QPO and LFN processes are in fact completely due to random noise processes, as suggested by van der Klis (1989*b*), power fluctuations in these components are present and quantifiable in the statistical aggregate with the present signal to noise strength of ~ 0.5.

b) Search for Fluctuation Correlations: The Split Power Test

The existence of QPO and LFN power fluctuations suggests that a search for correlations between the two can be performed by dividing 1 s power spectra into two subsamples: spectra with high or low QPO powers, or alternatively, spectra with high or low LFN powers. Some of the spectra in which QPO (LFN) power deviates from the average power per frequency channel will merely reflect statistical fluctuations. However, Figures 4*b* and 4*d* give estimates of the maximum degree of correlation to expect (assuming that some part of the signal is deterministic). For instance, if a high/low QPO dichotomy is constructed by selecting powers at 24 Hz, as much as $\sim 20\%$ of the QPO power fluctuations above a power of 7 might be found to be associated with LFN fluctuations; the actual percentage would depend upon the degree of correlation. In principle, a very low degree of correlation could be detected with a large enough data set. We proceed to describe the application of this split power test to GX 5−1 and the simulated data sets using QPO or LFN frequency and power band selector criteria.

We performed split power tests in which the QPO was the selector using frequency bands 1, 3, and 5 Hz wide centered on 24 Hz, and power discriminator levels from 5 to 9 units. Figure 5*a* illustrates a typical result: the power spectrum with the tall QPO peak was generated by averaging individual spectra with any occurrence of QPO power in the three-channel band 23–25 Hz greater than 7 units (*open circles*), while all spectra with no occurrence greater than 7 in that band comprise the average with the lower QPO peak (*filled squares*). There is no significant corresponding differential in the LFN peaks or in the LFN spectral shape. Similarly, when LFN is the power selector, no significant difference is observed between the two averaged spectra in the QPO bump, as illustrated in Figure 5*b* where channels 1–6 Hz with powers greater than 10 units are the discriminator. For each variant on the split power test—band width, power discriminator level, combined, low-, or high-energy data sets—a null correlation was found. Table 2 summarizes some of these results for GX 5−1. Entries in Table 2 are ratios of power above and below the discriminator level for both the selector band and the other band. The power ratios for the selector band are always significantly greater than unity, as expected. For GX 5−1, the power ratio for the other band is always consistent with unity.

The simulated data sets were constructed to have varying degrees of correlation between LFN and QPO amplitude so that we might quantify the meaning of the null results for GX 5−1. The amount of correlation depends primarily on shot rate and secondarily on shot shape. The models are named according to these parameters. Model E100 has *exponential* shot shapes, R100 has *rectangular* shot shapes, and both have 100 Hz shot rates. Figures 5*c* and 5*d* illustrate results of the split power test for model R28I, constructed such that occurrences and amplitudes of LFN shots and QPOs are *independent* (this is the only model in the present paper in which shots do not carry the QPO). Like GX 5−1, no correlation is evident. The contrasting results of the split power test for shot model R28 are shown in Figures 5*e* and 5*f*. At low enough shot rates the relationship between LFN and QPO is

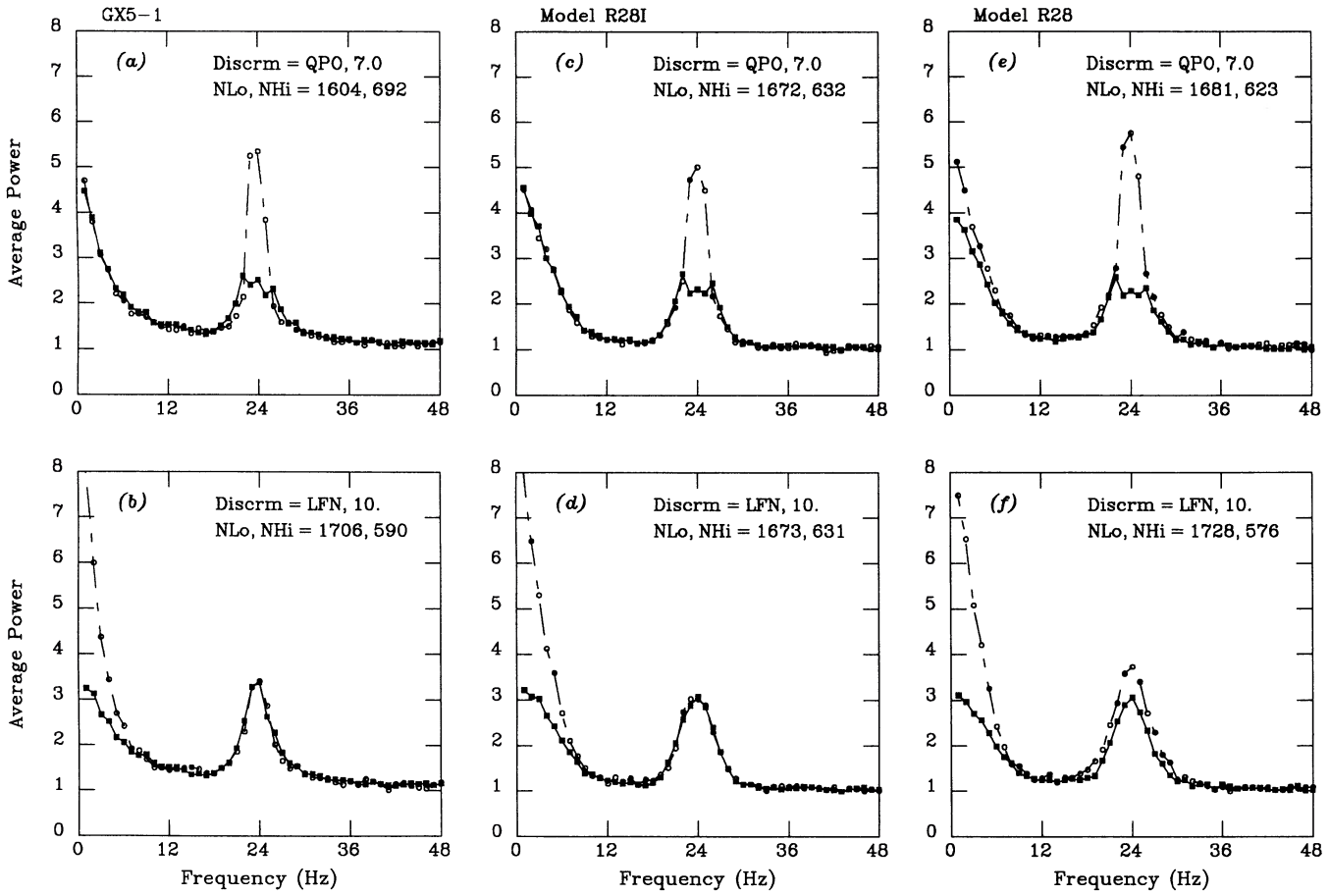

FIG. 5.—Split power test: dichotomy of averaged power spectra, above (*open circles*) and below (*filled squares*) discriminator power level. QPO selection band: 22.5–25.5 Hz; LFN band: 0.5–6.5 Hz. (*a–b*) GX 5−1 data for QPO, LFN as selector, Models R281 (*c, d*) and R28 (*e, f*) for same.

clearly revealed by the split power test on a 1 s time scale. Positive correlations for model R28 are evident when either LFN or QPO is the selector band, as can be seen from the differing peak heights for the other band.

Power ratios from the split power test for some of the models are also given in Table 2. As the shot rate increases, the power ratio in the other band approaches unity to within errors; this is the leveling effect of the intrinsic noise bias (in addition to the extrinsic noise bias of photon counting statistics). For model R100 the test is significant at the ~ 2–$3\,\sigma$ level, depending on the discriminator band and power level. At 400 Hz shot rates, both the exponential and rectangular

TABLE 2

TEST OF QPO, LFN CORRELATION

LEVEL	BAND (Hz)	BAND POWER RATIO: ABOVE/BELOW FILTER LEVEL				
		GX 5−1	Model R400	Model R100	Model R28	Model E400
QPO Filter						
5.0	1–6	0.97 ± 0.02	1.01 ± 0.03	1.07 ± 0.03	1.25 ± 0.03	1.01 ± 0.03
	23–25	3.67 ± 0.17	4.15 ± 0.20	4.20 ± 0.20	4.89 ± 0.24	4.02 ± 0.18
7.0	1–6	0.99 ± 0.03	1.00 ± 0.03	1.09 ± 0.03	1.32 ± 0.04	1.01 ± 0.03
	23–25	2.93 ± 0.11	3.41 ± 0.14	3.33 ± 0.14	3.79 ± 0.15	3.22 ± 0.13
9.0	1–6	1.00 ± 0.03	1.01 ± 0.04	1.09 ± 0.04	1.33 ± 0.04	0.95 ± 0.04
	23–25	2.76 ± 0.12	3.27 ± 0.16	3.21 ± 0.15	3.61 ± 0.16	3.09 ± 0.15
LFN Filter						
8.0	23–25	1.07 ± 0.04	0.99 ± 0.04	1.08 ± 0.04	1.36 ± 0.05	0.98 ± 0.04
	1–6	2.27 ± 0.06	2.43 ± 0.06	2.29 ± 0.06	2.51 ± 0.06	2.36 ± 0.06
10.0	23–25	1.05 ± 0.04	1.00 ± 0.04	1.11 ± 0.05	1.38 ± 0.06	1.01 ± 0.05
	1–6	2.18 ± 0.06	2.32 ± 0.06	2.24 ± 0.06	2.40 ± 0.06	2.26 ± 0.06

models are consistent with no correlation—the constructed relationship is masked for 1 s integrations. Therefore, with the amount of data utilized, this test precludes the possibility of LFN shots carrying the QPO in GX 5−1 for shot rates less than ~100 Hz.

c) *Third Moment Test: Skewness*

Other statistical tests may be performed which yield information concerning the LFN and QPO shape distributions and the distribution of LFN waveforms relative to the local mean. Skewness, the third moment of the intensity distribution of the time series, may be defined.

$$\mathrm{Sk} = (1/N) \sum_i [(I(t_i) - \mu)/\sigma]^3 , \quad (3)$$

where $I(t_i)$ is the count rate time series, μ is the mean, σ the standard deviation, and N the number of samples. Note that for this definition skewness has no dimensionality. Unlike σ, Sk does not scale with the mean. Skewness and moments of higher order characterize the degree to which a distribution departs from a normal one, thus measuring its shape. Skewness describes the asymmetry of the data about the mean. For reference, Sk for a negative rectified sinusoid (i.e., $-|\sin x|$), is $+\frac{1}{2}$.

Skewness of real and simulated data sets reflects the convolution of several factors. The low count rates of data sets with shorter time scale binning will have positive Sk merely because the distribution is Poissonian rather than Gaussian. If the data were exactly Poisson distributed then the expected skewness would be

$$\mathrm{Sk}_{\mathrm{Pois}} = \sum_n \left(\frac{n-\mu}{\sigma}\right)^3 \frac{e^{-\mu}\mu^n}{n!} = \mu^{-1/2} , \quad (4)$$

and the formal error would be

$$\epsilon_{\mathrm{skew}} = [(1/N) \sum (\mathrm{Sk} - \mathrm{Sk}_{\mathrm{Pois}})^2]^{1/2} = [(15 + 24/\mu + 1/\mu^2)/N]^{1/2} . \quad (5)$$

Note that as $\mu \to \infty$, $\mathrm{Sk}_{\mathrm{Pois}} \to 0$, as expected for a normal distribution. The actual error in the skewness determination will depend upon the degree to which the data depart from a Poisson distribution on a given time scale and can be several times ϵ_{skew}. Note that equation (3) is insensitive to temporal ordering, and therefore many non-Poissonian distributions with differing phase relationships between Fourier components can manifest similar skewness.

The QPO and LFN are examples of non-Poissonian components. For the generic case in which LFN is a manifestation of shots, if all shots had unit amplitude, unit width, rectangular shape, and uniformly distributed start times, then the resulting skewness of the piled up shots would be Poissonian. For data in which amplitude, width, and shape distributions are present, the resulting skewness becomes a complicated function of these quantities. Also, from equation (3) we see that skewness is nonlinear: contributions from separate components do not simply add to give total skewness. If the QPO component is not sinusoidal, then the skewness is further altered on the relevant time scale. Measurement factors such as dead time may enter the equation on shorter time scales as well. Finally, components of skewness on long time scales contribute to short time scale skewness measurements, but not vice versa since short time-scale waveforms are lost when binned up above characteristic periods. All these considerations must be taken into account when attempting to interpret skewness determinations.

We computed the skewness of GX 5−1 and the simulated data sets on time scales ranging from 2 ms to 1 s. The results are summarized in Table 3. The errors quoted in Table 3 are from equation (5). Empirical errors were estimated by computing skewness for fractions of each data set. For GX 5−1 the skewness is significantly less than that of a Poisson distribution on time scales ~62 to 16 ms. On longer (LFN) time scales, skewness is still below that of Poisson noise, but not very significantly. It is likely that finite binning and/or dead time effects account for the excess skewness at 2 ms (and possibly they affect the measurement at 8 ms); since Fourier power above the QPO band is nearly Poissonian, we do not expect an appreciable deterministic component at high frequency which would contribute to the skewness. Therefore, we conclude that the waveforms present on time scales ranging from shorter than the QPO period (<40 ms) to near the coherence length (~100 ms) have some asymmetrical, negative skewness shape, whereas LFN shapes on longer time scales are approximately equally distributed about the mean intensity level. Methods for estimating the characteristic shape near the QPO time scale are briefly discussed in § IV.

In contrast, all the positive-only shot models which fit the average GX 5−1 power spectrum exhibit significant positive skewness on time scales 250 ms or less. For models with higher shot rate the (monotonic) trend is lower (but still significant) skewness. The trend is more complex for variations in shot shape. At low shot rates rectangular models manifest higher skewness than exponential models (compare R100 and E100, ≥62 ms) because the latter have long tails which, when overlapped, produce a smoother LFN component (the contribution to skewness of tails overrides that of spikes). However, for exponential shots the distribution of LFN lifetimes must be lowered as shot rate increases in order to fit the GX 5−1 LFN

TABLE 3

SKEWNESS ON QPO AND LFN TIME SCALES

Time Scale	Poisson Noise	GX 5−1	Model R400	Model R100	Model R28	Model E400	Model E100	Formal Error[a]
2 ms	0.242	0.266	0.295	0.311	0.343	0.297	0.315	±0.004
8 ms	0.121	0.113	0.247	0.315	0.454	0.252	0.328	±0.007
16 ms	0.086	0.039	0.244	0.334	0.553	0.231	0.362	±0.010
31 ms	0.061	0.031	0.196	0.260	0.460	0.172	0.282	±0.014
62 ms	0.043	−0.057	0.176	0.243	0.445	0.153	0.231	±0.020
125 ms	0.030	−0.011	0.178	0.228	0.409	0.151	0.212	±0.029
250 ms	0.021	−0.028	0.115	0.210	0.350	0.140	0.136	±0.040
1 s	0.011	−0.012	0.152	0.277	0.311	0.013	0.046	±0.081

[a] Error for Poisson-distributed data. Empirical errors are comparable to formal errors; see text.

e-folding frequency scale (more exponential spikes, more high frequency content, therefore longer lifetimes required; see Table 1). Thus, less pile-up results and skewness increases, becoming comparable to that in rectangular models (compare R400 and E400, ≥ 62 ms). The trend is for skewness to increase on shorter (QPO) time scales. This must be attributed to the effect of piled up shots since the QPOs themselves are constructed to be sinusoidal.

We note that to first order the small fluctuations in the mean of the GX 5−1 data do not influence the global skewness; as can be seen from equation (3), variations of order 2% on a several second time scale should produce little effect. We verified that this is the case by computing the skewness with and without low frequency filters applied to the data (8 and 16 s rectangular smooths). Smoothing has a minor effect on time-scales from 62 ms to 1 s, shifting the skewness closer to the Poisson noise values by approximately the magnitude of the quoted errors. For the simulated data sets, there is no corresponding effect since the mean on a time scale of several seconds more closely tracks the global mean.

We conclude that the lack of significant skewness in GX 5−1 on time scales longer than ~ 100 ms is inconsistent with rectangular or exponential shots. This conclusion is actually more general since skewness is insensitive to time ordering. For instance, bi-exponential shots (with both exponential rise and decay) on the quoted time scale are also excluded. Table 3 shows that such skewness should be detected for shot rates up to ~ 400 Hz, although shot rates much higher than 400 Hz may be consistent with our results. The limit on shot rate is somewhat dependent on shot shape; however, we see from the above discussion that at high shot rates the piling up of shots is a more important factor in total skewness than the shape of individual shots.

d) Correlation of LFN with Average Flux: Local Mean Test

We have seen that the skewness test for GX 5−1 implies that the LFN shape distribution is nearly symmetrical about the mean. Since some variation in shot rate must occur, intervals with many positive-only shots would enhance the local intensity more than intervals with few shots, regardless of shot shape. Thus we may generalize the skewness results by searching for a correlation between LFN power and local mean on a 1 s time scale in both GX 5−1 and the shot model simulations. This test is similar to the split power test except that a dichotomy of local mean distributions is computed for occurrences of LFN power above and below a given discriminator level.

The GX 5−1 data were first convolved with a 16 s wide rectangle function (i.e., a running average) since some intensity variation is present (see Fig. 2) which is either intrinsic to the source or due to collimator modulation. Collimator movement occurs on time scales of minutes, and therefore its effects should be eliminated by the 16 s smooth, whereas intrinsic source variations on a ~ 1 s time scale are preserved. Figure 6*a* illustrates the result of the test for GX 5−1. The LFN dis-

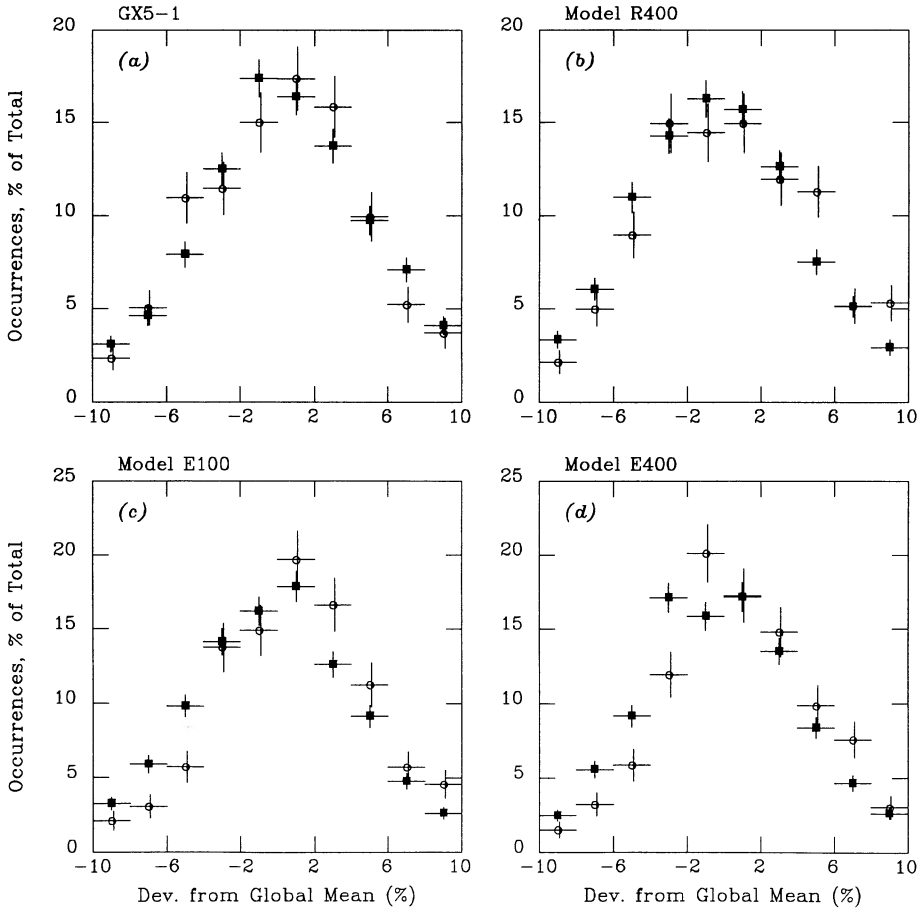

FIG. 6.—Distribution of local (1 s time scale) mean intensities selected by LFN power. Above (*open circles*) and below (*filled squares*) discriminator power level of 10 units. LFN selection band: 0.5–6.5 Hz. (*a*) GX 5−1 data and (*b–d*) models R400, E100, and E400.

criminator power level is 10 units for the LFN band 1–6 Hz. The local mean distributions associated with high (*open circles*) and low (*filled squares*) LFN powers do not show any significant relative shift. A similar result is obtained when the test is performed on the data without the smooth. Thus the local mean test corroborates the skewness test for GX 5–1 in that no evidence for positive-only shots is found. In fact, for a "split spectra" test where local mean is the discriminator, the average power spectra computed for occurrences of local mean either above or below the global mean are indistinguishable, within errors, in the LFN band.

The results of the local mean versus LFN power test for some shot models are also shown in Figures 6*b*–6*d*. The expected positive correlation which arises from variations in the number of overlapping shots is evident from the relative shift of the local mean distributions. The difference is significant in each case, albeit less pronounced for the higher shot rate models. Therefore, with this test we can discern (random) variations in the shot rate for positive-only LFN shots at shot rates as high as 400 Hz and probably somewhat higher, at least in the 1–6 Hz LFN component.

The lack of a positive correlation between LFN and local mean in the GX 5–1 data, and the clear presence of such correlations in simulations with shot rates up to ~400 Hz, implies that, for any shot model to be viable, the shot rate of positive-only LFN shots in GX 5–1 must exceed ~400 Hz, or that a second component of negative shots with comparable strength must be present.

We also considered a test for correlation between local mean and QPO power. van der Klis *et al.* (1985) first showed for GX 5–1 that as the source intensity increases, the QPO power peak diminishes while it broadens, and the QPO centroid frequency increases. Even though the source intensity is relatively stable in this observation, local mean variations of a few percent in source intensity make these effects in the QPO band perceptible in a "split spectra" test. Therefore, a test for correlation between local mean and QPO power might yield results with ambiguous interpretation.

However, we would expect that the corresponding effect for the local mean versus LFN power should be more nearly negligible since the change in the LFN component with intensity is approximately half that in the QPO for the same intensity variation (§ II*a*), and since the LFN power is distributed (and measured) over a wider bandwidth. In fact, as stated previously the shape of the average spectra *in the LFN band* are indistinguishable for GX 5–1 spectra grouped on the basis of the local mean.

IV. DISCUSSION

In this article we have primarily addressed the questions: Is there an association between LFN and QPO in GX 5–1 on the horizontal branch, in that LFN shots are the envelope of the QPO? Are positive-only shots responsible for a significant component of the LFN power? In view of the low S/N of the QPO, a range of simulations were performed in order to calibrate the sensitivity of our tests to possible correlations in the real data.

For GX 5–1 the split power test yields no indication of correlation between the QPO and LFN components on time scales near 1 s. By itself, the split power test for this observation is not sensitive enough to rule out a QPO–LFN relationship for shot rates higher than ~100 Hz. Nevertheless, in principle, the sensitivity of the split power test increases with the integration time and therefore may provide more stringent limits when applied to larger data sets. This test provides a straightforward conceptual example of the kinds of statistical tests of QPO shot models which are possible. A similar test using an optimal linear filter is superior since it probes time scales comparable to the QPO coherence length and nearer the rapid fluctuations of intrinsic noise bias introduced by many overlapping shots. Preliminary results from this test indicate that the QPO–LFN relationship can be distinguished in model simulations with shot rates at least as high as 400 Hz (Norris *et al.* 1990).

The moment tests performed on GX 5–1 and shot model simulations strongly suggest that positive-only shots are not operating in GX 5–1 for shot rates at least as high as 400 Hz. In GX 5–1 the intensity skewness vanishes on LFN time scales, within errors, suggesting that the distribution of LFN shapes at frequencies 1 Hz or greater is symmetrical about the mean. Furthermore, no correlation between local mean and LFN power is observed. Results for shot model simulations show that for shot rates up to ~400 Hz, the piling up of shots gives rise to positive skewness and a correlation of local mean with LFN power.

It might be possible to construct physical models with positive-only shots such that the skewness vanishes, e.g., with negative skewness shape distributions for individual shots. However, for the BFMA model still to be viable, the null result for the local mean test requires that two LFN components in the range 1–6 Hz operate, one being a positive amplitude shot component (perhaps associated with the QPOs) and the other, a negative amplitude component with a similar distribution. With this arrangement a symmetric (zero skewness) LFN would result.

Another possibility not excluded by our analysis is that the shots responsible for the QPOs have lifetimes longer than ~1 s. This seems counterintuitive, however, since in the BFMA model context we would expect LFN envelopes with lifetimes of approximately the QPO coherence length (two to three cycles, ~0.1 s) to carry the QPOs. For the LFN band from 1 to 10 Hz not to be associated with the QPOs would require some

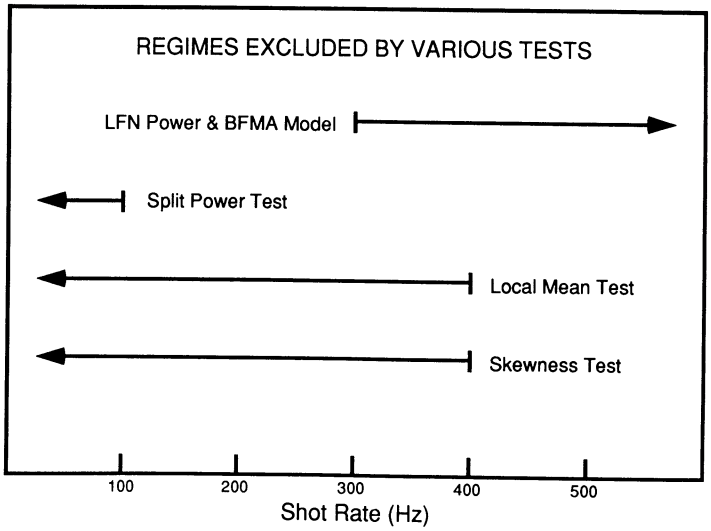

FIG. 7.—Shot rate regimes excluded by split power, skewness, and local mean vs. LFN power tests, compared to regime excluded by BFMA sinusoidal model. See text.

sort of exclusionary principle which is not postulated by the BFMA model (Lamb *et al.* 1985; Shibazaki and Lamb 1987).

Figure 7 summarizes our results, comparing the range of excluded shot rates for the three statistical tests with the range excluded by the BFMA model of Lamb *et al.* (1985). We follow their argument to obtain an upper limit on the number of shots resident simultaneously in the magnetospheric transition region, and then assuming a characteristic time scale for shots to traverse the region, we derive an approximate upper limit on the shot rate. The total mean intensity is the sum of the steady component, I_0, and the contribution of the average number of simultaneous shots, $\langle N \rangle$,

$$\langle I \rangle = I_0 + \langle N \rangle \langle A \rangle = (f+1)\langle N \rangle \langle A \rangle , \quad (6)$$

where $\langle A \rangle$ is the average amplitude per shot and I_0 has been expressed as a fraction of the shot component. The normalized power in the LFN component is

$$\gamma^2_{\rm LFN} = P_{\rm LFN}/P_0 = 0.5\langle N \rangle \langle A^2 \rangle / \langle I \rangle^2 \quad (7)$$

(where, as in Lamb *et al.*, two is the spectral normalization, rather than unity as in the rest of this paper). For $\langle A^2 \rangle = \langle A \rangle^2$ and $\gamma_{\rm LFN} = 0.13$, corresponding to an rms fractional intensity of the GX 5−1 LFN of ~6% (see van der Klis *et al.* 1985), equations (6) and (7) yield

$$\langle N \rangle = 0.5[\gamma_{\rm LFN}(1+f)]^{-1/2} \simeq 30/(1+f)^2 . \quad (8)$$

If *none* of the luminosity arises from a steady component, $\langle N \rangle \simeq 30$; else $\langle N \rangle < 30$. This agrees with the limit derived by Lamb *et al.* (1985) for an approximately sinusoidal QPO, which is implied by the absence of a conspicuous first harmonic in the average GX 5−1 power spectrum (Fig. 2). Values for $\langle N \rangle$ which agree with Lamb *et al.* (1985) are discussed in Lamb (1986) and Shibazaki and Lamb (1987). These authors are misquoted by Lamb (1989), who is apparently referring to shot rates of ~200–3000 s^{-1} (the former value being applicable to the sinusoidal BFMA model), rather than $\langle N \rangle$ itself. The shot rate is

$$R_{\rm shot} = \langle N \rangle / \tau_{\rm trans} , \quad (9)$$

where $\tau_{\rm trans}$ is the time for shots to cross the transition region. This is much longer than the free-fall time (~1 ms), since the clumps of accreting matter describe quasi-Keplerian orbits. A plausible value for $\tau_{\rm trans}$ is the QPO coherence length of two to three cycles, ~100 ms. At ~100 km from the neutron star, 6 Keplerian orbits in the transition region is ~100 ms, during which time a few QPO beat periods would occur. These values are also close to the average lifetime of LFN shots in some models. Thus an estimate for $R_{\rm shot}$ is ~300 Hz or less for the BFMA sinusoidal model.

The shot rate limit provided by the skewness test assumes that individual shots have approximately zero skewness; shots with negative skewness could give rise to a total resultant skewness of approximately zero. However, the limit imposed by the local mean test is independent of shot shape; random variations in shot rate are discernible with this test for average shot rates up to 400 Hz by their contribution to the local mean. This is a difficulty which must be solved for the BFMA (sinusoidal) model to remain viable. Either shot rates higher than 300 Hz must somehow operate, giving rise to a larger intrinsic noise bias, or a separate negative shot component must be present.

The BFMA model was originally advanced to explain the correlation of QPO centroid frequency with X-ray intensity in GX 5−1 (Alpar and Shaham 1985; Lamb *et al.* 1985). An important consequence of the theory is that it also required a correlation of LFN and QPO strengths, which is observed on intermediate time scales of minutes (van der Klis *et al.* 1985). In an analysis performed using standard correlation techniques, Mitsuda *et al.* (1990) find that the QPO–LFN strength correlation develops on time scales longer than ~8 s, corroborating our result for GX 5−1. Thus, it is possible that QPOs and LFN at frequencies ~1 Hz and higher are only phenomenologically connected by a third parameter, for instance, accretion rate.

We note that inclusion of possible effects such as QPO coherence across shots, QPO amplitude decay, timing correlations, and other features can mask the relationship between QPO and LFN in the BFMA context (Shibazaki and Lamb 1987; Shibazaki, Elsner, and Weisskopf 1987; Elsner, Shibazaki, and Weisskopf 1987). We do incorporate the important feature of QPO coherence across shots—shot clustering—which lessens the correlation with LFN. In fact, it is necessary to include some shot clustering in order to fit the narrowness of the QPO peak, unless LFN on time scales longer than 1 s is predominantly responsible for carrying the QPO. We note that these additional theoretical effects are not relevant to the constraint provided by the local mean test, which is insensitive to LFN shape.

Additional progress on the question of the QPO–LFN relationship can be made by using algorithms which explore the QPOs on shorter time scales near the coherence length. Also, theory could be better constrained with knowledge of attributes such as the average pulse shape which gives rise to QPOs, the relationship between adjacent pulses, and spectral hardness as a function of pulse phase. These problems can be successfully pursued in the statistical aggregate using available data—if proper account is taken of the large noise bias. We suggest the use of time domain analysis techniques such as autoregressive–moving average models (Scargle 1981; 1990) and optimal linear filters (Norris *et al.* 1989*b*, *c*) for probing QPO shape, phase relationships, and duty cycle. For instance, optimal filter algorithms can be used to probe directly the QPO coherence length distribution, and search for frequency modulation and phase mode switching (Norris *et al.* 1989*a*, *b*).

We thank Noriaki Shibazaki and Freb Lamb for enlightening conversations. We also thank the referee, Michiel van der Klis, for several insightful comments. This work was supported by the Office of Naval Research and the National Aeronautics and Space Administration.

REFERENCES

Alpar, M. A., and Shaham, J. 1985, *Nature*, **316**, 239.
Elsner, R. F., Shibazaki, N., and Weisskopf, M. C. 1987, *Ap. J.*, **320**, 527.
Groth, E. J. 1975, *Ap. J. Suppl.*, **29**, 285.
Hasinger, G., Langmeier, A., Sztajno, M., Trumper, J., Lewin, W. H. G., and White, N. E. 1986, *Nature*, **319**, 469.
Hasinger, G., and van der Klis, M. 1989, *Astr. Ap.*, in press.
Lamb, F. K. 1986, in *The Evolution of Galactic X-Ray Binaries*, ed. J. Trumper, W. H. G. Lewin, and W. Brinkmann (Dordrecht: Reidel), p. 151.
Lamb, F. K. 1988, *Adv. Space Res.*, **8**, 421.
———. 1989, in *Proc. 23rd ESLAB Symposium*, ed. J. Hunt and B. Battrick (Noordwijk: ESA), p. 224.
Lamb, F. K., Shibazaki, N., Alpar, M. A., and Shaham, J. 1985, *Nature*, **317**, 681.
Leahy, D. A., *et al.* 1983, *Ap. J.*, **266**, 160.
Lewin, W. H. G., van Paradijs, J., and van der Klis, M. 1988, *Space Sci. Rev.*, **46**, 273.

Makino, M. 1987, *Ap. Letters Comm.*, **25**, 223.
Mitsuda, K., Dotani, T., Yoshida, A., Vaughan, B. A., and Norris, J. P. 1990, *Pub. Astr. Soc. Japan*, in press.
Norris, J. P., Hertz, P., Wood, K. S., Vaughan, B. A., Michelson, P. F., Mitsuda, K., and Dotani, T. 1989*a*, *Bull. A.A.S.*, **21**, 749.
———. 1989*b*, *Bull. A.A.S.*, **21**, 1209.
———. 1989, *Proc. 23rd ESLAB Symposium*, ed. J. Hunt and B. Battrick (Noordwijk: ESA), p. 557.
Scargle, J. D. 1981, *Ap. J. Suppl.*, **45**, 71.
———. 1990, *Ap. J.*, submitted.
Shibazaki, N., Elsner, R. F., and Weisskopf, M. C. 1987, *Ap. J.*, **322**, 831.
Shibazaki, N., and Lamb, F. K. 1987, *Ap. J.*, **318**, 767.
Stella, L. 1988, *Adv. Space Res.*, **8**, 367.
Turner, M. J. L., *et al.* 1989, *Pub. Astr. Soc. Japan*, **41**, 345.
van der Klis, M. 1986, in *Lecture Notes in Physics*, Vol. **266**, p. 157. *The Physics of Accretion onto Compact Objects*, ed. K. O. Mason, M. G. Watson, and N. E. White (Berlin: Springer-Verlag), p. 157.
———. 1988, *Adv. Space Res.*, **8**, 383.
———. 1989*a*, *Ann. Rev. Astron. Ap.*, **27**, 517.
———. 1989*b*, in *Timing Neutron Stars*, ed. H. Ogelman and E. P. J. van den Heuvel (Dordrecht: Kluwer), p. 27.
van der Klis, M., Jansen, F., van Paradijs, J., Lewin, W. H. G., van den Heuvel, E. P. J., Trumper, J., and Sztajno, M. 1985, *Nature*, **316**, 225.

P. HERTZ, J. P. NORRIS, and K. S. WOOD: Code 4120, Naval Research Laboratory, Washington, DC 20375-5000

P. F. MICHELSON and B. A. VAUGHAN: Physics Department, Stanford University, Stanford, CA 94305

T. DOTANI and K. MITSUDA: Institute for Space and Astronautical Science, 1-1, Yoshinodai 3-chome, Sagamihara-shi, Kanagawa, Japan